

# Vortex phase diagram in rotating two-component Bose-Einstein condensates

Kenichi Kasamatsu<sup>1</sup>, Makoto Tsubota<sup>1</sup>, and Masahito Ueda<sup>2</sup>

<sup>1</sup>*Department of Physics, Osaka City University, Sumiyoshi-Ku, Osaka 558-8585, Japan*

<sup>2</sup>*Department of Physics, Tokyo Institute of Technology, Meguro-ku, Tokyo 152-8551, Japan*

(Dated: February 7, 2020)

We investigate numerically the structure of vortex states in rotating two-component Bose-Einstein condensates with equal intracomponent but varying intercomponent coupling constants. A phase diagram in the intercomponent-coupling versus rotation-frequency plane reveals rich equilibrium structures of vortex states. As the ratio of intercomponent to intracomponent couplings increases, the interlocked vortex lattices undergo phase transitions from triangular to square, to double-core lattices, and eventually phase-separate to spontaneously develop interwoven vortex sheets with each component made up of chains of singly quantized vortices.

PACS numbers: 03.75.Lm, 03.75.Mn, 05.30.Jp

A quantized vortex lattice in a rotating trapped Bose-Einstein condensate (BEC) has been observed by several groups[1]. Although most experiments have been conducted with single-component BECs, richer phenomena are expected in rotating two-component BECs consisting, for example, of two different hyperfine spin states of atoms [2]. The two-component BECs are described by two different macroscopic wave functions. This system has three coupling constants denoted by  $C_{11}$  and  $C_{22}$  (for intracomponents), and  $C_{12}$  (for intercomponent), which give rise to nontrivial static and dynamical properties not found in a single-component BEC [3, 4, 5, 6, 7]. A system described by a multicomponent order parameter can excite various exotic topological defects. There have been growing interests in the study of unconventional topological defects in the field of multicomponent superfluids and superconductors, providing us with an ideal testing ground to investigate closely related problems in high-energy physics and cosmology. In this Letter, we report equilibrium structures of vortex states in two-component BECs with  $C_{11} = C_{22} = C$  under external rotation by the numerical analysis of the Gross-Pitaevskii equation.

Recently, Mueller and Ho studied the vortex lattice structure of two-component BECs by assuming the lowest Landau level approximation and a perfect lattice [8]. They proposed a phase diagram on the lattice structure; as the intercomponent interaction is increased, positions of vortex cores in one component are shifted from those of the other, and the structure changes continuously from triangular to square lattices. Kita *et al.* discussed the lattice structure in  $F = 1$  spinor BECs [9]. However, both studies assume the rotation frequency to be close to the radial trapping frequency, so a vast experimentally accessible parameter regime remains to be explored. Because of the repulsive intercomponent interaction, two components tend to repel each other. When there is no external rotation, we obtain miscible condensates as the ground state for  $C_{12}/C < 1$ , while for  $C_{12}/C > 1$  the two components phase separate [3, 4, 7]. We will show that the same conclusion holds in the equilibrium state

under rotation, too. The present numerical analysis reveals a rich variety of vortex structures which have eluded the analytic treatment. We find triangular lattices and square lattices for  $C_{12}/C < 1$ , and double-core vortex lattices and vortex sheets for  $C_{12}/C \geq 1$  to be stable for considerable range of rotation frequency; these states are observable in current experimental situations.

The equilibrium solutions of two-component BECs in harmonic potentials  $V_i$  are obtained by solving the time-independent coupled Gross-Pitaevskii equations for the macroscopic wave functions  $\Psi_i$  ( $i = 1, 2$ ) [3, 4, 5, 6, 7],

$$(h_i + \sum_{j=1,2} C_{ij} |\Psi_j|^2) \Psi_i = \mu_i \Psi_i \quad (1)$$

with  $h_i = -(m_{12}/m_i) \nabla^2 + V_i - (\Omega/\bar{\omega}) L_z$ . These equations have been normalized by using  $\hbar\bar{\omega} \equiv \hbar(\omega_1 + \omega_2)/2$  as the energy unit and  $b_{ho} = \sqrt{\hbar/2m_{12}\bar{\omega}}$  as the length unit, where  $m_{12} = m_1 m_2 / (m_1 + m_2)$  represents the reduced mass. The centrifugal term  $(\Omega/\bar{\omega}) L_z = i(\Omega/\bar{\omega})(y\partial_x - x\partial_y)$  appears in a system rotating about the  $z$  axis. In this work, the numerical calculation is done in the two-dimensional  $x - y$  space. We assume that the wave functions are normalized as  $\int dx dy |\Psi_i(x, y)|^2 = 1$ . Then, the intra- and intercomponent coupling constants are written as  $C_{ii} = 8\pi(m_{12}/m_i) N_i^{2D} a_{ii}$  and  $C_{ij} = 4\pi N_j^{2D} a_{12}$  ( $i \neq j$ ) with the corresponding s-wave scattering lengths  $a_{11}$ ,  $a_{22}$ ,  $a_{12}$  (assumed to be positive), and the particle numbers  $N_i^{2D}$  per unit length along the  $z$ -axis.

For simplicity, the number of the parameters is reduced by assuming  $a_{11} = a_{22}$ ,  $m_1 = m_2$  and  $\omega_1 = \omega_2 = \bar{\omega}$ , and  $N_1^{2D} = N_2^{2D} = N^{2D}$ . For the typical experimental conditions  $(\omega_\perp, \omega_z) = 2\pi(8, 5)\text{Hz}$  and  $N \sim 10^6$ , the values of the intracomponent coupling constants are chosen as  $C_{11} = C_{22} = C = 2000$ . In the numerical calculation, the equilibrium solutions are found by the norm-preserving imaginary time propagation of the time-dependent version of Eq. (1), starting from arbitrary trial wave functions without vorticity. The propagation continues until the fluctuation in the norm of the wave function becomes smaller than  $10^{-8}$ .

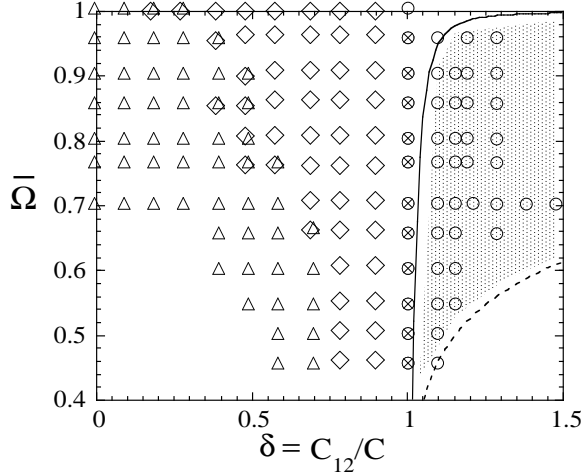


FIG. 1:  $\bar{\Omega}$ - $\delta$  phase diagram of the vortex states in rotating two-component BECs. The classification of the structure is made by the symbols,  $\triangle$ : triangular lattice,  $\diamond$ : square lattice,  $\otimes$ : stripe or double-core vortex lattice,  $\circ$ : vortex sheet. Because of the continuous change from triangular to square, their boundary is shown by using both  $\triangle$  and  $\diamond$ . The plots at  $\bar{\Omega} = 1$  show the results of Ref. [8]. The shaded region is analytically obtained region of vortex sheets; the solid curve represents  $b = \Lambda_p$  and the dashed curve  $2b = R_{TF}$  (see text).

With a fixed value  $C = 2000$ , we investigate the equilibrium solutions for various values of two free parameters  $\delta \equiv C_{12}/C$  and  $\bar{\Omega} \equiv \Omega/\bar{\omega}$ . The obtained vortex structure is summarized in the phase diagram of Fig. 1. The upper limit of the rotation frequency is  $\bar{\Omega} = 1$ , because the centrifugal potential overcomes the harmonic trapping potential for  $\bar{\Omega} > 1$ . Some previous studies have revealed that two irrotational components with equal mass and equal intracomponent scattering length overlap completely for  $\delta < 1$ , and phase-separate for  $\delta > 1$  [3, 4, 7]. This criterion is reflected on the structure of vortex states, as explained below. In general, there are many metastable states in rotating two-component BECs; they are obtained by the numerical simulation starting from different wave functions. Here we discuss some characteristic features of vortex structures.

In the overlapping region  $\delta < 1$ , two types of the regular vortex lattices are obtained as the equilibrium state. For  $\delta = 0$  where two components are not interacting, the formulation is equivalent to that of one component, thereby triangular vortex lattices being formed [10]. As  $\delta$  increases, the positions of vortex cores in one component gradually shift from those of the other component and the triangular lattices are distorted. Eventually, the vortices in each component form a square lattice rather than a triangular one. The  $\delta$  dependence on the stable region of a square lattice was studied in Ref. [8] under the rapidly rotating limit  $\bar{\Omega} \simeq 1$ . As seen in Fig. 1, however, that stable region depends on not only  $\delta$  but also  $\bar{\Omega}$ . The

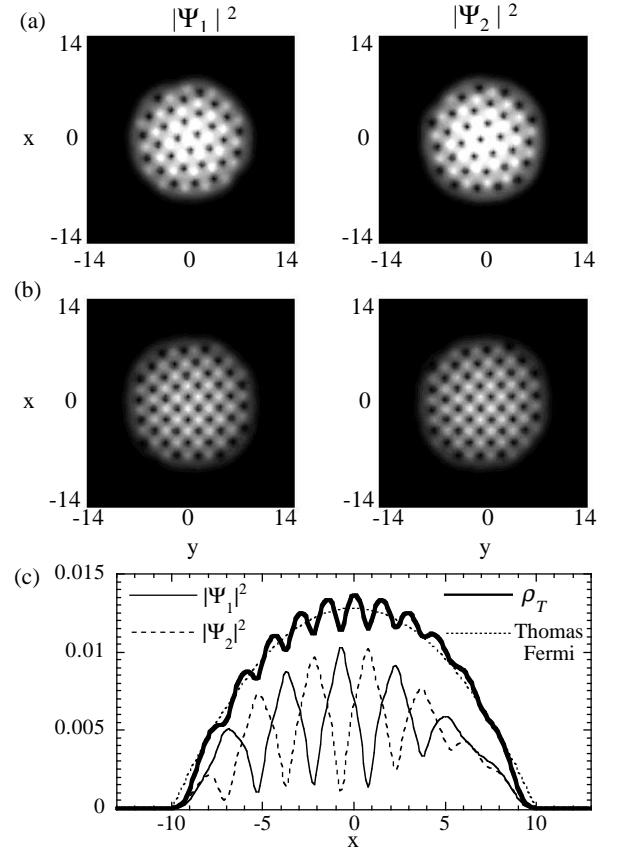


FIG. 2: Two-dimensional density profile of the condensates with  $C = 2000$  and  $\delta = 0.7$  for (a)  $\bar{\Omega} = 0.6$  and (b)  $\bar{\Omega} = 0.75$ . (c) Cross section of (b) along the  $y = 0$  line. The total density  $\rho_T = |\Psi_1|^2 + |\Psi_2|^2$  and the Thomas-Fermi density profile are also shown.

increase of rotation frequency also causes the transition from triangular to square lattices; in Figs. 2 (a) and (b), the two-dimensional density profiles of the condensates with  $\delta = 0.7$  are shown for  $\bar{\Omega} = 0.6$  and  $\bar{\Omega} = 0.75$ . We find that the two vortex lattices are interlocked in such a manner that a peak in the density of one component is located at the density hole of the other, as shown in Fig. 2 (c). As a result, the total density  $\rho_T = |\Psi_1|^2 + |\Psi_2|^2$  obeys the Thomas-Fermi distribution applied to the overlapping two-component BECs with solid-body rotation  $\rho_T(r) = 2\sqrt{\alpha/\pi} - \alpha r^2$  with  $\alpha = (1 - \bar{\Omega}^2)/C(1 + \delta)$ . We have confirmed that this feature holds for other parameter regimes.

Why is the square lattice stabilized in two-component BECs? According to the energy functional of this system, two components interact via the intercomponent interaction  $C_{12}|\Psi_1|^2|\Psi_2|^2$ ; the velocity field in one component is independent of that of the other. Therefore, such a feature is determined *only by the density distribution of the condensates* which minimizes the interaction energy. We rewrite the interaction energy in terms of the total

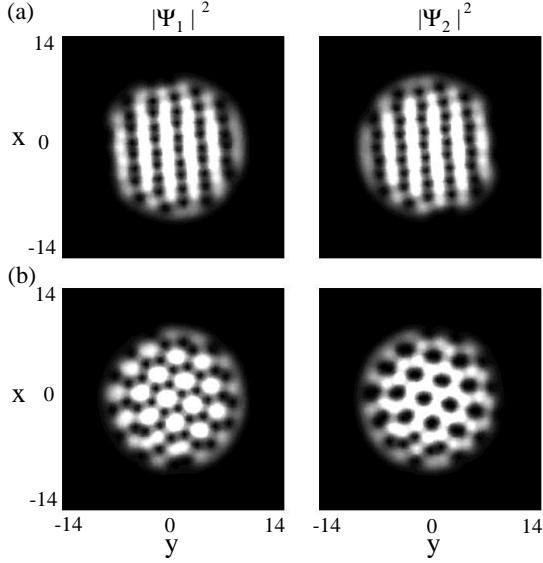


FIG. 3: The density profiles of the condensates  $\Psi_1$  and  $\Psi_2$  for  $\bar{\Omega} = 0.7$  and  $\delta = 1$ . The profiles (a) and (b) are obtained by the numerical simulation starting from different trial wave functions. The energy difference between these states is  $\Delta E \sim 10^{-5}$ .

density  $\rho_T$  and the “spin” variable  $S = |\Psi_1|^2 - |\Psi_2|^2$  as

$$E_{\text{int}} = \int d\mathbf{r} \frac{C}{4} \left[ (1 + \delta) \rho_T^2 + (1 - \delta) S^2 \right]. \quad (2)$$

A larger  $\delta$  makes a smoother total density  $\rho_T$  more favorable in order to reduce the first term of Eq. (2). This results in the shift of the positions of vortex cores of each component. Then, the last term of Eq. (2) can be interpreted effectively as the interaction energy between spins in the Ising model [11]. Spin-up components correspond to the density peaks of  $\Psi_1$  at the vortex cores of  $\Psi_2$ , and vice versa for spin-down components. When the coefficient  $1 - \delta$  is positive, the interaction between spins is anti-ferromagnetic, which makes a square lattice stabilized (because the triangular lattice could be frustrated). As both  $\delta$  and  $\bar{\Omega}$  increase, the interlocking of vortex lattices becomes stronger, anti-ferromagnetic nature being made more pronounced. Therefore, owing to the interlocking of vortex lattices, the rotating two-component BECs can be described by the Ising model.

As  $\delta$  exceeds unity, the system enters a ferromagnetic phase. Then, the condensates undergo phase separation to spontaneously form domains having the same spin component [11]. Concurrently, vortices begin to overlap at  $\delta \sim 1$ . Figure 3 shows typical solutions at  $\delta = 1$ . In Fig. 3(a), vortices of each component are overlapped in lines, and each condensate density forms a stripe pattern. Note that the vortex stripes reported in Ref. [12] appear in a nonequilibrium situation in the presence of quadrupolar perturbation. While this structure can also be derived if one assumes a perfect lattice [8], we note

that its energy is nearly degenerate with that of Fig. 3(b). For the same parameters, we can obtain another equilibrium state called “double-core vortex lattice” in Fig. 1, where a vortex lattice of component 2 is made by pairs of vortices with the same circulation; vortices in component 1 surround those pairs. Therefore, various metastable structures will be observed in this parameter region.

For strongly phase-separated (ferromagnetic) region  $\delta > 1$ , the density peaks of the same spin component, at which the other-component vortices are located, merge further, resulting in the formation of vortex sheets; a typical example is shown in Fig. 4(a). Singly quantized vortices line up in sheets, and the sheets of component 1 and 2 are interwoven alternately from the center to the outward. Figure 4(b) shows that each superfluid velocity  $v_i$  ( $i = 1, 2$ ) jumps at the vortex sheet, following approximately the velocity of solid-body rotation. In the region  $\delta > 1$ , even though the value of  $\delta$  is changed, the total density is fixed by the Thomas-Fermi distribution with  $\delta = 1$ .

The stationary vortex sheet has been observed in rotating superfluid  $^3\text{He-A}$  [13], where vortices are bounded to a topologically stable domain wall soliton across which the unit vector representing the direction of the orbital angular momentum of the Cooper-pair faces oppositely. As discussed in superfluid  $^3\text{He-A}$ , the equilibrium distance between the sheets of component 1 and component 2 is determined by the competition between the surface tension  $\sigma$  of the domain wall and the kinetic energy of the superflow [13]. In order to estimate that distance in two-component BECs, we consider a simple model shown in Fig. 4(c). In this model, each velocity is assumed to be constant between the vortex sheets of the *same* component; the value of  $v_i$  increases by  $2\bar{\Omega}b$  across every sheet. The total density  $\rho_T = |\Psi_1|^2 + |\Psi_2|^2$  is constant, and the domain boundary with the penetration depth  $\Lambda$  is approximated by the linear profile. We calculate the free energy  $F = E - \Omega L_z$  in the range  $0 < r < 2b$ , the sheet distance  $b$  being determined so as to minimize  $F$  per unit area. Firstly, the penetration depth  $\Lambda$  is determined by minimizing the surface tension  $\sigma$  of a single domain wall with respect to  $\Lambda$  [7], which is the sum of the quantum pressure energy  $E_{\text{qp}}/2\pi b \approx (\rho_T/2\Lambda)$  and the interaction energy in the overlap region  $E_{\text{int}}/2\pi b = (\delta - 1)\Lambda\rho_T^2/12$ ; we thus obtain  $\Lambda_p = \sqrt{6/C(\delta - 1)\rho_T}$ . Then, the surface tension is written as  $\sigma = \rho_T^{3/2} \sqrt{C(\delta - 1)/6}$ . Secondly, the flow energy per area (in rotating frame) is given by  $(1/4\pi b^2) \int_0^{2b} d^2r \sum_i \rho_i (v_i - \bar{\Omega}r)^2/2 = 29\rho_T\bar{\Omega}^2 b^2/768$ , where  $b \ll \Lambda_p$  is assumed. Thus, the free energy per unit area is written as

$$\frac{F}{4\pi b^2} = \frac{29\rho_T\bar{\Omega}^2 b^2}{768} + \frac{2\sigma}{b} + \frac{C\rho_T^2}{2}. \quad (3)$$

Minimizing this energy with respect to  $b$ , one obtains  $b = (768\sigma/29\bar{\Omega}^2\rho_T)^{1/3} = (768/29\bar{\Omega}^2\Lambda_p)^{1/3}$ . By using the

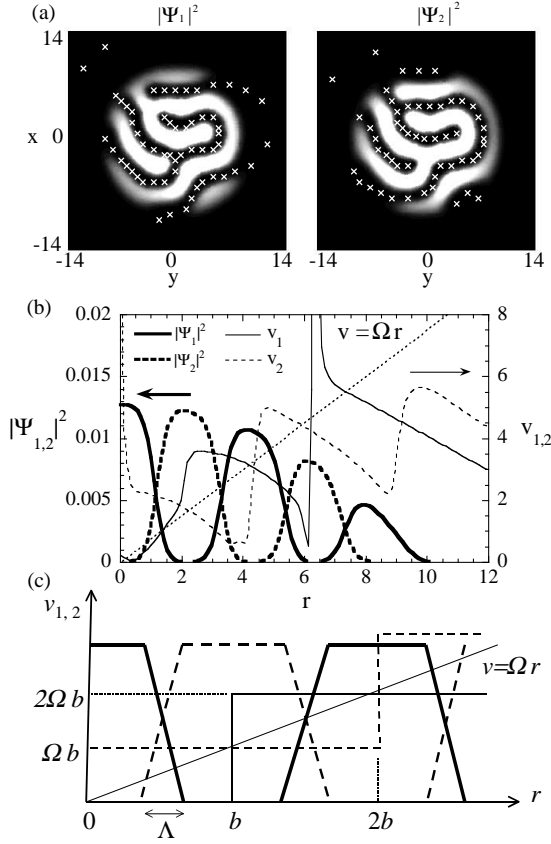


FIG. 4: (a) The density profiles of the condensates for  $\bar{\Omega} = 0.75$  and  $\delta = 1.1$ . The vortex sheets are made up of chains of singly quantized vortices whose positions are marked by  $\times$ . (b) The density profile of  $\Psi_1$  and  $\Psi_2$  in the radial component, and the corresponding velocity profile. The velocity of solid-body rotation is shown by the dotted line. (c) Schematic illustration of the model of the vortex sheet state.

Thomas-Fermi density at  $r = 0$  with  $\delta = 1$  as the value of  $\rho_T$ , the sheet spacing  $b \propto (\delta - 1)^{1/6} (1 - \bar{\Omega}^2)^{1/12} / \bar{\Omega}^{2/3}$  is consistent with that of numerical solutions; for example, for parameters used in Fig. 4 we obtain  $b = 3.09b_{ho}$ . The vortex sheet is expected in the region  $b > \Lambda_p$  and  $2b < R_{TF} = \sqrt{2/\sqrt{\pi\alpha}}$ , as shown in the shaded region in Fig. 1. When  $2b > R_{TF}$ , i.e.,  $b$  becomes comparable with the condensate size, the clear structure of sheets vanishes.

Finally, we comment on what structure could be observed in actual experimental conditions. The two-component BECs realized in JILA is a mixture of the states  $|1, -1\rangle$  and  $|2, 1\rangle$  of  $^{87}\text{Rb}$ . This mixture has the scattering lengths which have the same order,  $a_{11} : a_{22} : a_{12} = 1 : 0.94 : 0.97$ , i.e.,  $\delta \sim 1$  for equal particle numbers. Therefore, lattices with partially overlapping vortices, as shown in Fig. 3, are expected to be observed. Using  $^{85}\text{Rb}|2, 2\rangle$  atoms is fascinating because both the intercomponent scattering length and the scattering length

of  $^{85}\text{Rb}|2, 2\rangle$  can be controlled by using Feshbach resonance. A mixture of  $^{41}\text{K}$  and  $^{87}\text{Rb}$  BECs which is reported recently [14] lies deeply in a phase-separate region. The vortex sheets should therefore be observed at high rotation frequencies.

In conclusion, numerical simulations of stable vortex lattice structures in two-component BECs reveal a rich phase diagram of vortex state, even in the restricted parameter space  $(\delta, \bar{\Omega})$ . Use of different atomic masses and intracomponent interactions will realize a coexistence system of vortices with different vortex-core size; such a situation may change the lattice structure shown in this Letter. We plan to study a more detailed phase diagram, and formation dynamics of vortex lattices in multicomponent BECs.

- 
- [1] K.W. Madison *et al.*, Phys. Rev. Lett. **84**, 806 (2000); J.R. Abo-Shaer *et al.*, Science, **292**, 476 (2001); P.C. Haljan *et al.*, Phys. Rev. Lett. **87**, 210403 (2001); E. Hodby *et al.*, Phys. Rev. Lett. **88**, 010405 (2002).
  - [2] C.J. Myatt, E.A. Burt, R.W. Ghrist, E.A. Cornell, and C.E. Wieman, Phys. Rev. Lett. **78**, 586 (1997).
  - [3] T.-L. Ho and V.B. Shenoy, Phys. Rev. Lett. **77**, 3276 (1996).
  - [4] B.D. Esry, C.H. Greene, J.P. Burke, Jr. and J. L. Bohn, Phys. Rev. Lett. **78**, 3594 (1997).
  - [5] P. Öhberg and S. Stenholm, Phys. Rev. A **57**, 1272 (1998).
  - [6] H. Pu and N.P. Bigelow, Phys. Rev. Lett. **80**, 1130 (1998).
  - [7] E. Timmermans, Phys. Rev. Lett. **81**, 5718 (1998).
  - [8] E.J. Mueller and T.-L. Ho, Phys. Rev. Lett. **88**, 180403 (2002).
  - [9] T. Kita, T. Mizushima, and K. Machida, Phys. Rev. A **66**, 061601(R) (2002).
  - [10] M. Tsubota, K. Kasamatsu, and M. Ueda, Phys. Rev. A **65**, 023603 (2002).
  - [11] The energy Eq. (2) is analogous to that of a binary alloy, in which  $N/2$  A atoms and  $N/2$  B atoms are distributed on  $N$  lattice sites. At each site there is only  $n_{Ai}$  or  $n_{Bi}$  ( $n_i = 0$  or 1) atom. Denoting the three kinds of interaction energies between the atoms as  $\epsilon_A$ ,  $\epsilon_B$ , and  $\epsilon_{AB}$ , the interaction energy of this system reads  $\sum_{i,j} \{ \epsilon_A n_{Ai} n_{Aj} + \epsilon_B n_{Bi} n_{Bj} + \epsilon_{AB} (n_{Ai} n_{Bj} + n_{Aj} n_{Bi}) \}$ . The replacement  $s_i = n_{Ai} - n_{Bi}$  reduces this energy to  $\text{const} + \epsilon \sum_{i,j} s_i s_j$ . When the coefficient  $\epsilon = (\epsilon_A + \epsilon_B + \epsilon_{AB})/4 > 0$ , the interaction is anti-ferromagnetic, while for  $\epsilon < 0$ , it is ferromagnetic. See, for example, K. Huang, *Statistical Mechanics*, 2nd ed. Chap. 14 (Wiley New York, 1987).
  - [12] P. Engels, I. Coddington, P.C. Haljan, and E.A. Cornell, Phys. Rev. Lett. **89**, 100403 (2002).
  - [13] Ü. Parts, E.V. Thuneberg, G.E. Volovik, J.H. Koivu-niemi, V.M.H. Ruutu, M. Heinilä, J.M. Karimäki, and M. Krusius, Phys. Rev. Lett. **72**, 3839 (1994).
  - [14] G. Modugno, M. Modugno, F. Riboli, G. Roati, and M. Inguscio, Phys. Rev. Lett. **89**, 190404 (2002).